Estimation method for errors of an aerostatic planar *XY* stage based on measured profiles errors

Jooho Hwang · Chun-Hong Park · Seung-Woo Kim

Abstract This paper describes a method for estimating the geometric errors of an aerostatic planar *XY* stage. The method calculates two-dimensional (2D) position errors and flatness based on measured guideway profiles. Profile measurements, estimates of motion error, and geometric error models are considered to estimate the 2D position and flatness errors along the *X*- and *Y*-axes. A three-probe system is used to measure the guideway profiles for the *X*- and *Y*-axes. The motion errors, which are used as input data for geometric error models, are calculated from the force equilibrium of aerostatic bearings along the measured guideway profiles and compared with laser interferometer measurements. Geometric error models were derived to calculate the 2D position and flatness errors of the stage. The measured results and estimates for the 2D position error and flatness differed by 0.5 and 0.6 μm, respectively. Therefore, the proposed estimation method for 2D position and flatness errors of an aerostatic planar *XY* stage will be a useful tool during the machining and assembly of guideways.

J. Hwang (✉) · C.-H. Park
Intelligent Manufacturing System Research Division,
Korea Institute of Machinery and Materials,
171 Jang-dong,
Yuseong-Gu, Daejeon 305-343, South Korea
e-mail: jooho@kimm.re.kr
URL: http://www.kimm.re.kr

C.-H. Park
e-mail: pch657@kimm.re.kr
URL: http://www.kimm.re.kr

S.-W. Kim
School of Mechanical Engineering, Korea Advanced Institute
of Science and Technology,
373-1 Gusung-dong,
Yuseong-Gu, Daejeon 305-751, South Korea
e-mail: swk@kaist.ac.kr
URL: http://pem.kaist.ac.kr

1 Introduction

A planar *XY* stage is frequently used as a precision positioning system for equipment that produces semi-conductors or flat panel displays [1, 2]. Thus, higher velocities and better accuracies are required to attain higher productivity and performance measures. A planar *XY* stage, for which an H-shaped frame is usually used as the base stage, is driven by two actuators, such as linear motors, with two position feedback sensors, such as linear scales or interferometers on the scanning motion axis [3, 4]. The stage is frequently used as the main frame of the equipment, and the machining and assembly process of the rails and bed of the stage is one of first processes performed when the equipment is built [5]. The two-dimensional (2D) position, motion, and stage flatness errors are measured when the system is tested after it is complete. If the stage errors do not meet the required specifications, the stage must be remachined and the assembly process must be repeated. This is difficult and time-consuming work, especially when the assembly and disassembly process must be repeated for a large stage.

In this paper, a method to estimate the errors of a planar *XY* stage is proposed that can be applied when the rails and bed of the stage are evaluated. The evaluation procedure requires three steps. First, the profiles of a pair of guide-ways are measured using a sequential two-point method and an extended reversal method. Then, the motion errors of the *X*- and *Y*-axes are estimated using the static equilibrium of an aerostatic bearing obtained from the

Fig. 1 Schematic diagram of an aerostatic planar *XY* stage

measured profiles. Finally, the 2D position and flatness errors are estimated using a homogeneous transformation matrix model from the estimated motion errors of the *X*- and *Y*-axes. The estimated results are compared to the 2D position and flatness errors obtained from the motion errors measured by a laser interferometer.

2 Configuration of the planar *XY* stage

A typical aerostatic planar *XY* stage was used to compare the estimated and experimental values. As shown in Fig. 1, the moving table of a planar *XY* stage translates along the *X*-axis on the base stage, which has an H-shaped structure and is driven by two simultaneously controlled linear motors (LM310-4, Trilogy) along the *Y*-axis. The stroke of each axis is 300 mm, which can be measured using a precise optical linear scale (LIP481, HeidenHain). A PC-based motion control board with a PID filter (PMAC2, Delta Tau) is used to control the position of the stage. The *X*- and *Y*-axes move on a granite bed, which is used as a vertical guide for the vacuum preloaded aerostatic bearings of the two stages to avoid deflections of the table and base stage and to reduce the moment forces in high acceleration motions. A double-pad aerostatic bearing is used to constrain the horizontal motion. As shown in Fig. 1, the base stage is constrained against the horizontal motion only at the aerostatic bearing on the Y_1 axis to avoid damages of the horizontal air bearings from thermal growth and parallel problems [5].

3 Guideway profile measurements

Guideways are important elements of an aerostatic planar *XY* stage. They usually consist of a pair of surfaces that provide a constraint in one direction, along with bearings, such as orifice or porous aerostatic bearings. The profiles of the pair of rails affect the straightness of the table and the clearance of the bearings affects the stiffness of the

guideways. A three-probe system [6], which consists of the reversal method [7–9] and the sequential two-point method [10–15], is used to measure the profiles of a pair of guideways.

A schematic diagram of the three-probe profile measurement system for a horizontal pair of rails is shown in Fig. 2. The probe stage, which carries the three probes and the angular optics of laser interferometer, moves along the pair of rails. The profiles of rail 1 and rail 2 are described by $f(\xi)$ and $g(\xi)$, respectively:

$$p_r(\xi_i) = m_1(\xi_i) + m_2(\xi_i) = f(\xi_i) - g(\xi_i)$$
$$f(\xi_i) \approx f_d(\xi_i) = f_d(\xi_{i-1}) + m_1(\xi_i) - m_3(\xi_i) + l\varepsilon_z(\xi_i) \quad (1)$$
$$g(\xi_i) \approx g_d(\xi_i) = f_d(\xi_i) - p_r(\xi_i)$$

where ξ is an arbitrary axis, which is actually the *X*- or *Y*-axis for planar *XY* stages, along the moving direction of the guideways; $m_1(\xi_i)$, $m_2(\xi_i)$, and $m_3(\xi_i)$ are the measured data of three displacement probes, P_1, P_2, and P_3, respectively; $\varepsilon_z(\xi_i)$ is the yaw error of the probe stage, which was measured by a laser interferometer (Agilent, 5529A Dynamic Calibrator User's Manual); l is the distance between P_1 and P_2, which was also the measuring step; and $f_d(\xi_i)$ is similar to $f(\xi_i)$, except that the initial measured values of $m_1(\xi_i)$ and $m_2(\xi_i)$ were set to 0 and the profile was calculated from incremental values; and $P_r(\xi_i)$ indicates the deviation of the two profiles along the *X*-axis or the parallelism of the pair of rails.

To measure the profiles of the rails for guideways that correspond to the *X*- and *Y*-axes, three inductive contact probes (Mahr, 1320/1) were used instead of noncontact probes, such as capacitive or eddy current probes, because the rails are made from undetectable materials, such as granite stone and anodized aluminum. An angular optic was fixed in the manual stage to measure the yaw errors of the stage, $\varepsilon_z(\xi_i)$, which had a displacement interferometer to detect its position, as shown in Fig. 3.
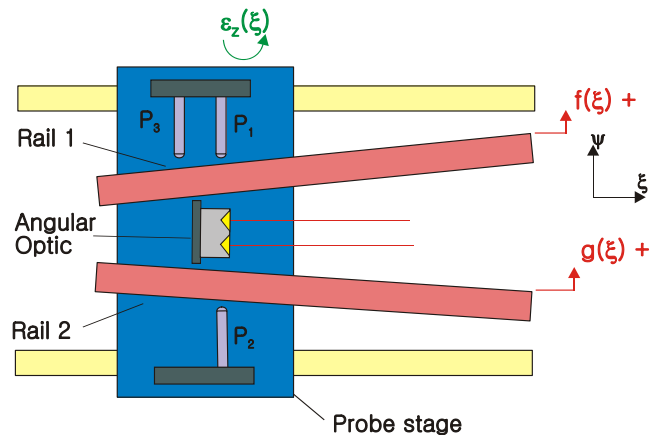
Fig. 2 Setup for measuring the profiles of a pair of rails
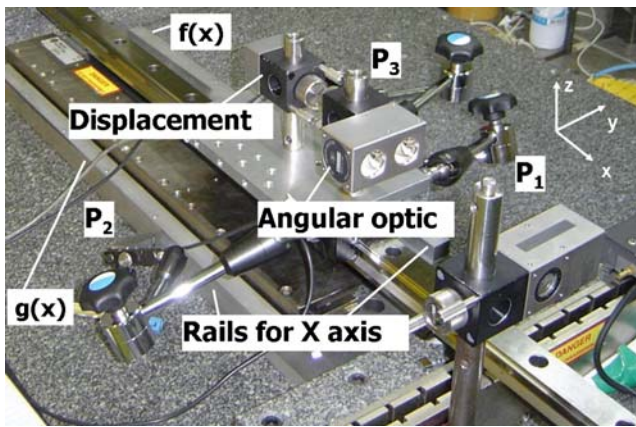
Fig. 3 Setup for measuring the profiles of a pair of X-axis rails

To simulate the influence of inductive sensors and setup errors, several error conditions were considered when describing the profiles of the pair of rails by Eq. 2, which is shown as a solid line in Fig. 4a:

$$f(\xi_i) = 6\sin\left(0.6\frac{\xi_i}{L}2\pi\right) + \sin\left(2\frac{\xi_i}{L}2\pi\right) + 0.03\xi_i$$
$$g(\xi_i) = 5\sin\left(0.6\frac{\xi_i}{L}2\pi\right) + 1.5\sin\left(3\frac{\xi_i}{L}2\pi\right) - 0.06\xi_i \quad (2)$$
$$e(\xi_i) = 3\sin\left(0.6\frac{\xi_i}{L}2\pi\right) + 0.01\xi_i$$

where $f(\xi)$ and $g(\xi)$ are the profiles of rails 1 and 2, respectively; L is the length of the rail in millimeter; and $e(\xi)$
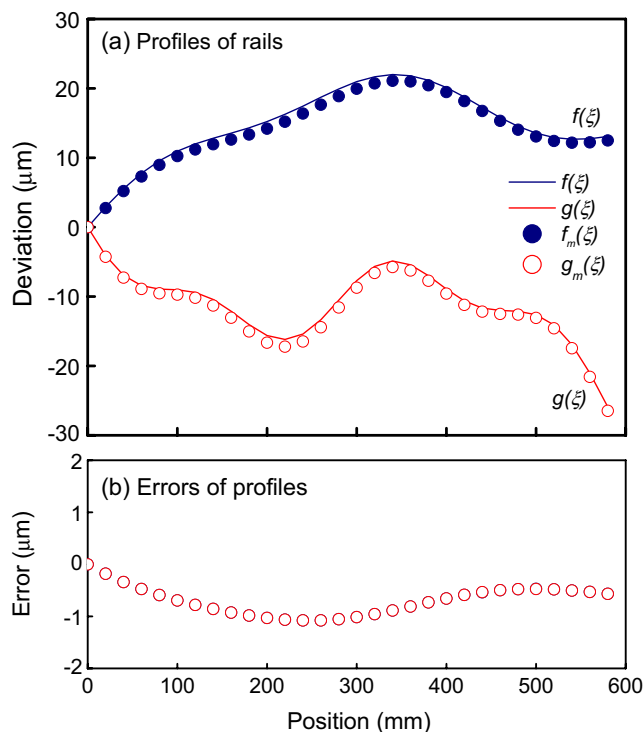
Fig. 4 Simulation results of the measured error due to a gain difference
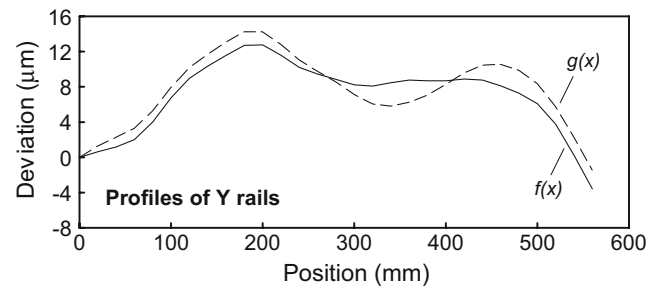
Fig. 5 Profiles of the Y-axis rails

is the motion error of the stage in micrometers due to straightness and alignment error, as shown in Fig. 2.

To keep the measuring error within 1 μm, which is 10% of the 10-μm clearance for aerostatic bearings, the following conditions are required: gain errors of less than 1% for P_1 and P_3, which are used to measure the straightness; a gain error of less than 4% for P_1 and P_2, which are used to measure the parallelism; a probe stage position error of less than ±3 mm; and a proven distance of less than ±0.5 mm. These values were obtained from a simulation of 600-mm-long rails defined by Eq. 2.

A comparison between the simulated measurements $(f_m(\xi), g_m(\xi))$ and a known pair of profiles $(f(\xi), g(\xi))$ is shown in Fig. 4a with 1% gain errors for P_1 and P_3. The error values are represented by circles in Fig. 4b. The errors of the two rails were the same and thus appear as one curve in the figure.

The profiles of each guideway measured using the method described above are shown in Figs. 5, 6, and 7. The guideways for the vertical direction of the X- and Y-axes were the surface of the bed. The vertical surface profiles were interpolated from the measured data shown in Fig. 7 to six different positions at which the center of the stage will be located during measurement of angular errors in Fig. 9a. To measure the vertical direction, the pitch errors of the probe stage were measured instead of the yaw errors described in Eq. 1.
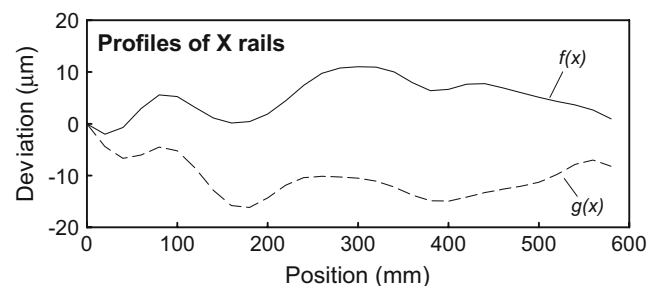
Fig. 6 Profiles of the X-axis rails
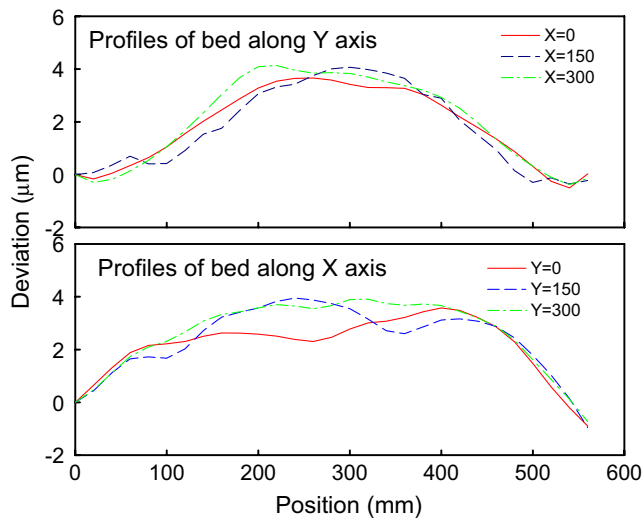
Fig. 7 Measured profile of the bed along the X- and Y-axes

4 Estimation of the motion errors

4.1 Static equilibrium model of the stage

A static equilibrium model is considered when calculating the motion errors of the stage along the measured profiles [16]. The static equilibrium model used to evaluate changes in the reaction force and displacement of a single pad of a porous aerostatic stage is shown in Fig. 8 where W is the external load of the table including its weight, m is the number of pads in the table, X_{ci} is the distance from the center of the table to the center of the pads, L is the length of the rails, and $F_i(x)$ and $z_i(x)$ are the ith reaction force and corresponding displacement of the center of the pads, respectively. The position of the center of the table is x and the slope of the table is $\theta(x)$.

If the relationship between the rail profiles and each pad of the table is considered, the pad of the table is moved to a new equilibrium state due to the changed aerostatic reaction force $f_{ei}(x)$ and new stage displacement $z_i(x)$; the reaction force is $F_i(x)$.

Assuming that the stiffness of the aerostatic pads is constant (K_0) within small displacements of the stage, the relationship between $f_{ei}(x)$ and $z_i(x)$ is:

$$f_i(x) = f_{ei}(x) - K_0 z_i(x). \tag{3}$$

Considering Eq. 3, the moment equilibrium from the reaction forces of the pads are:

$$\sum_{i=1}^{m} f_{ei}(x) - K_0 z_i(x) = 0, \tag{4}$$

$$\sum_{i=1}^{m} f_{ei}(x)\left(X_{ci} - R_i(x) + \frac{ml}{2}\right) = \sum_{i=1}^{m} K_0 z_i(x)\left(X_{ci} + \frac{ml}{2}\right)$$
$$x = \frac{ml}{2}, \cdots, L - \frac{ml}{2}. \tag{5}$$

The profiles of rails $e(x)$ can be represented as the Fourier transformed profiles:

$$e(x) = a_0 + \sum_{k=1}^{n}\left(a_k \cos\frac{2k\pi}{L}x + b_k \sin\frac{2k\pi}{L}x\right). \tag{6}$$

4.2 Computation of the motion error

The aerostatic bearing pads of the stage are of the same shape and have a multisupported configuration in the same plane, as shown in Fig. 8. Therefore, the error motion of the moving table of the stage can be calculated from the geometric relationship of each pad and the calculated characteristic of one pad. This can be determined quickly during the assembly process of the stage.

When a porous pad is moving along the rails and the center of the pad has the same coordinates as the rails, the profiles of the rails in Eq. 6 and the change of the reaction force of the porous pad $f_e(x)$ can be explained using the spatial frequency ω. The spatial frequency is defined as $\omega = 2\pi/\lambda$ where the wavelength for one sinusoidal profile of the rails is λ. When the wavelength is the same as the length of the pad l, the spatial frequency becomes $\omega_1 = 2\pi/l$. The change of the reaction force $f_e(x)$ has the same spatial frequency as the rails if the profile of the rail $e(x)$ has only a single spatial frequency ω. From this relationship, the motion transfer function may be defined as:

$$K(\omega) = \frac{f_e(\omega)}{e(\omega)}. \tag{7}$$

The linear and angular motions error can be represented by:

$$z(x) = \frac{1}{K_0 m}\sum_{i=1}^{m} f_e(x + X_{ci})$$
$$\theta(x) = \frac{12}{K_0 m(m^2-1)l^2}\sum_{i=1}^{m} f_e(x + X_{ci})X_{ci} - R_i(x + X_{ci}), \tag{8}$$
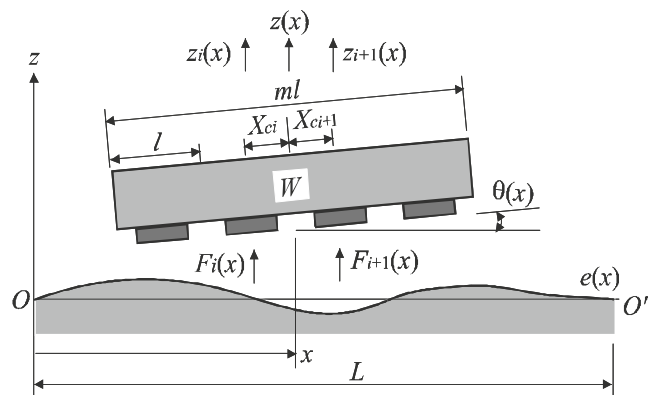
Fig. 8 Equilibrium state of a porous aerostatic stage

where $f_e(x)$ and $R(x)$ are:

$$f_e(x) = \sum_{k=1}^{n} K\left(\frac{2k\pi}{L}\right)\left(a_k \cos\frac{2k\pi}{L}x + b_k \sin\frac{2k\pi}{L}x\right) \quad (9)$$

$$R(x) = l\sum_{k=1}^{n} G\left(\frac{2k\pi}{L}\right)\left(a_k \cos\frac{2k\pi}{L}x + b_k \sin\frac{2k\pi}{L}x\right). \quad (10)$$

$$\begin{bmatrix} \delta P_x(i,j) \\ \delta P_y(i,j) \end{bmatrix} = \begin{bmatrix} -t_y\,\varepsilon_{z1}(j) + \varepsilon_{z2}(i) + t_z\varepsilon_{y2}(i,j) + \delta x_1(j) + \delta x_2(i) \\ t_x\,\varepsilon_{z1}(j) + \varepsilon_{z2}(i) - t_z\varepsilon_{x2}(i,j) + a_2(i)\varepsilon_{z1}(j) + a_2(i)\theta_{12} + \delta y_1(j) + \delta y_2(i) \end{bmatrix}. \quad (11)$$

In Eq. 11, each error motion contains an i or j index, or both. These are intermittent steps of the estimation and measurement process of the 2D error in the X- and Y-directions, respectively. The motion errors of the stage measured by the interferometer (HP5529A; Agilent, 5529A Dynamic Calibrator User's Manual), shown in Figs. 5, 6, and 7 and estimated by Eq. 8, are compared in Fig. 9. The yaw motion of base stage ε_{z1} is affected by the controlled position of the Y_1- and Y_2-axes. Therefore, the measured data of ε_{z1} were used to estimate the 2D position in both

The motion errors of the stage can be acquired from sequential repetitive calculations along the directions of motion.

5 Estimation of the 2D position and flatness errors

A 2D position error estimation model for a planar XY stage is derived for an aerostatic planar XY stage [17] based on a homogeneous transformation matrix [18–20]. It is represented by:

cases. As shown in Fig. 9, most of the motion errors were similar, but the yaw motion of the moving table along the X-axis had a slightly different shape.

The 2D position error of the stage was estimated from the sum of the motion errors every 10 mm over the 300× 300-mm translational area. The 2D position errors are compared in Fig. 10 for $t_x=0$ mm, $t_y=125$ mm, $t_z=60$ mm, and $\theta_{12}=0$. Interpolation was used to estimate the pitch errors $\varepsilon_{x2}(i,j)$ and $\varepsilon_{y2}(i,j)$, which had similar shapes at the three different measured positions because the position
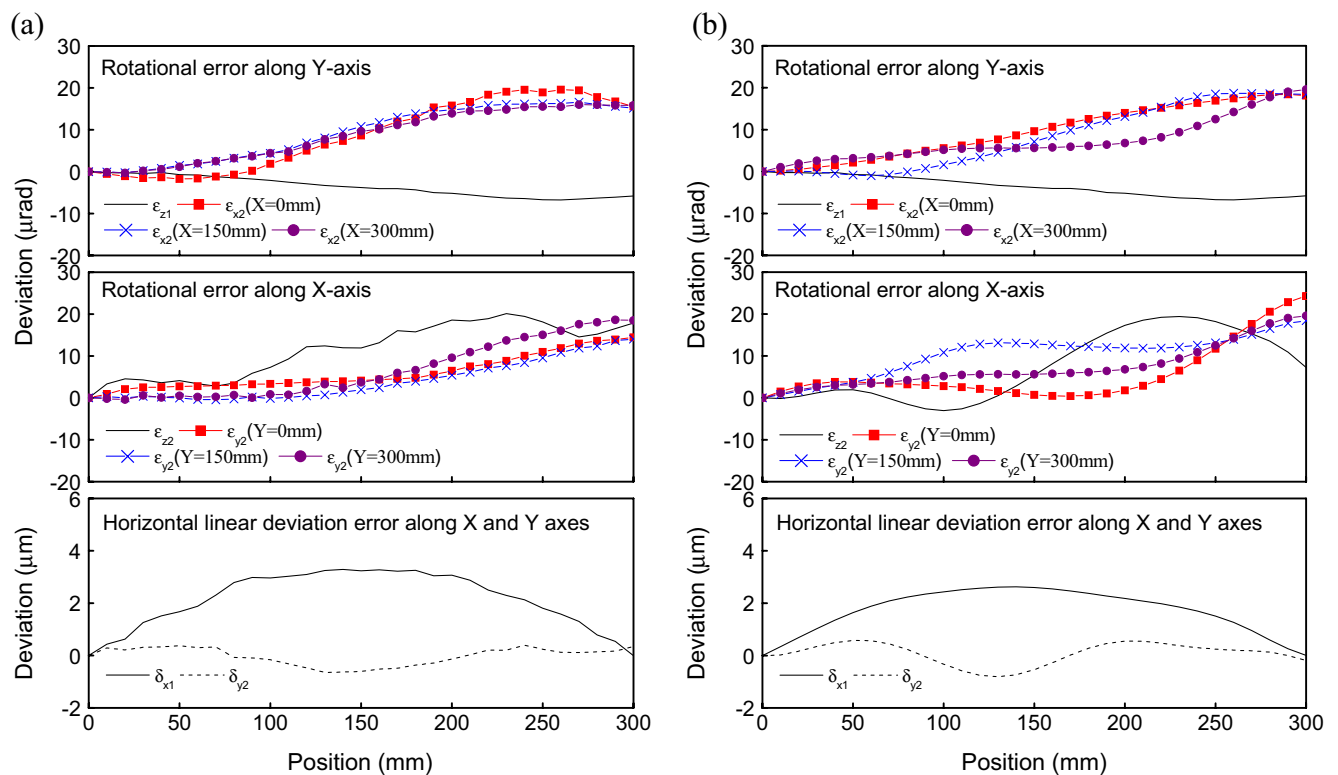
Fig. 9 Comparison between measured (a) and estimated (b) motion errors of the planar XY stage
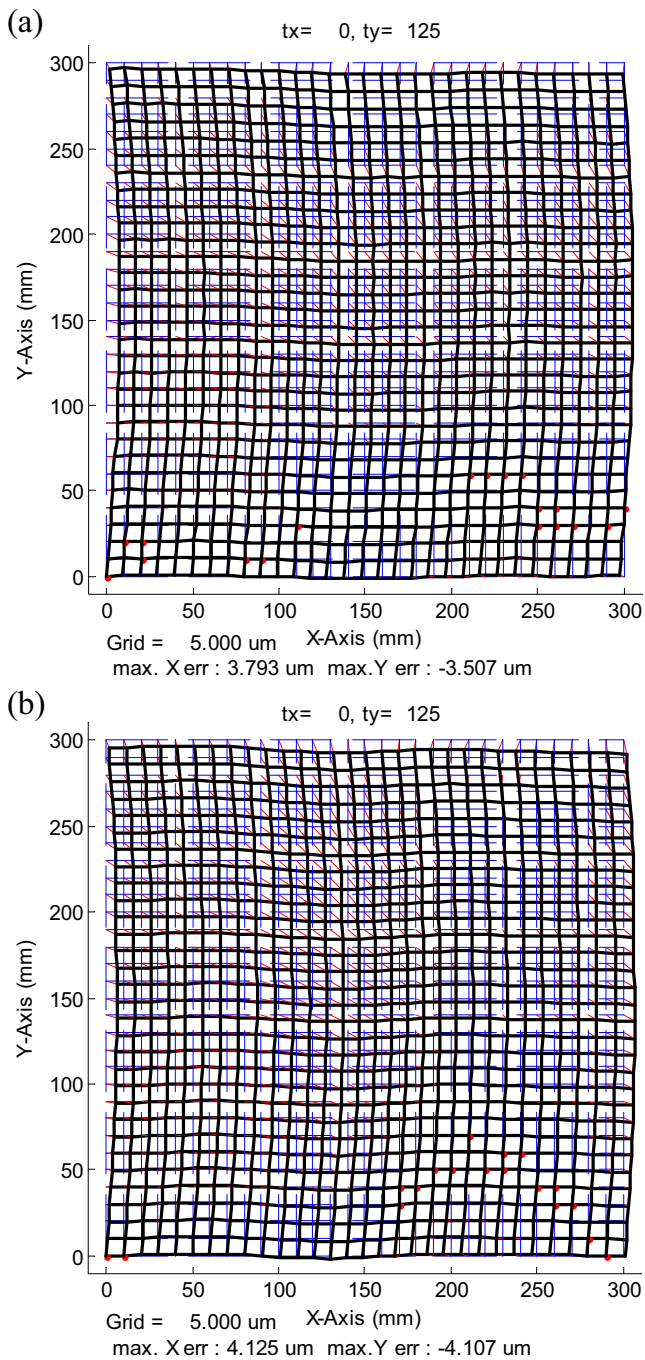
Fig. 10 Comparison between the measured (**a**) and estimated (**b**) 2D position errors at the center of the planar *XY* stage

difference of 150 mm was less than the span of the aerostatic bearings of the moving table, 270 mm. The maximum difference of the measured and estimated position errors was about 0.5 μm.

The straightness of the flatness can be calculated from summing each interpolated straightness data point, which can be measured directly or estimated from the measured profile data. A comparison of the flatness data is shown in Fig. 11. The maximum difference of the flatness error

between the measured and estimated values was about 0.6 μm. These results indicate that the proposed estimation method for 2D position errors and flatness on an aerostatic planar *XY* stage is useful in the machining and assembly process of guideways.

6 Conclusions

An estimation method was proposed for 2D position and flatness errors on an aerostatic planar *XY* stage. The error was estimated from an estimated motion error obtained using profile measurements of the guideways. Three steps were required to estimate the planar *XY* stage errors. First, the profiles of a pair of guideways were measured using a sequential two-point method and an extended reversal method. Then, the motion errors of the *X*- and *Y*-axes were estimated using the static equilibrium of the aerostatic bearing from the measured profiles. Finally, the 2D position and flatness errors were estimated using a homogeneous
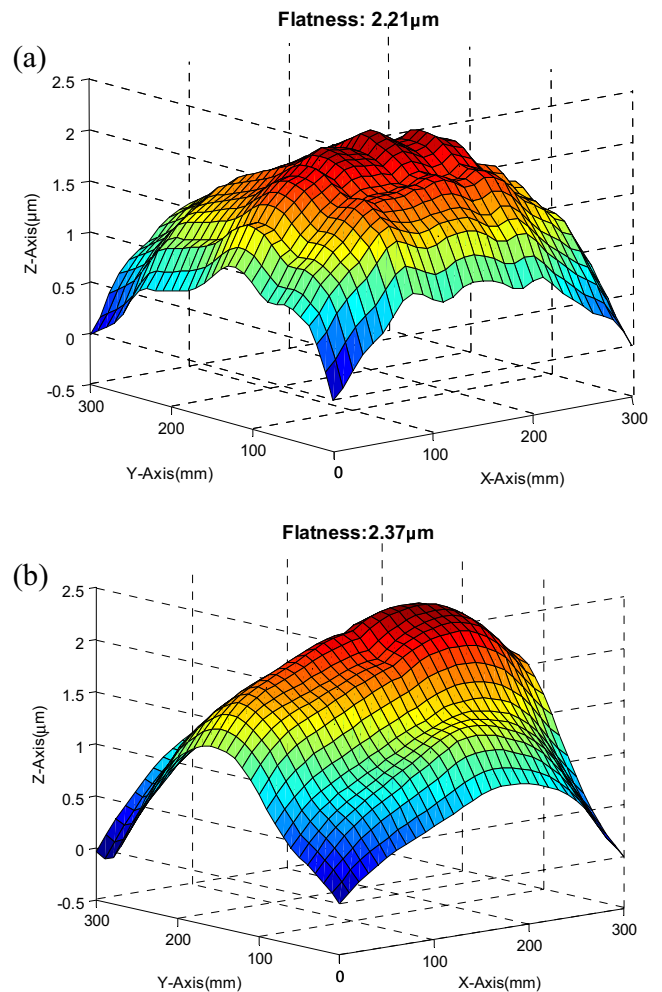
Fig. 11 Comparison between the measured (**a**) and estimated (**b**) flatness

transformation matrix model from the estimated motion errors of the *X*- and *Y*-axes. A comparison of experimental and estimated results demonstrated that the estimates were within 0.6 μm. Thus, the proposed estimation method for 2D position and flatness errors on an aerostatic planar *XY* stage can be successfully applied to evaluate the guideway of the aerostatic planar *XY* stage during the machining and assembly of guideways.

References

1. Lee C-W, Kim S-W (1997) An ultraprecision stage for alignment of wafers in advanced microlithography. Precis Eng 21:113–122
2. Kim W-J, Trumper DL, Bryan JB (1997) Linear motor-leviated stage for photolithography. CIRP Ann 46:447–450
3. Dejima S, Gao W, Shimizu H, Kiyono S, Tomita Y (2005) Precision positioning of a five degree-of-freedom planar motion stage. Mechatronics 15:969–987
4. Giam TS, Tan KK, Huang S (2006) Precision coordinated control of multi-axis gantry stages. ISA Trans 46:399–409
5. Novak WT, Premji Z, Nayak UG, Ebihara A (1997) Precision motion stage with single guide beam and follower stage. US patent 5,623,853
6. Hwang J, Park C-H, Gao W, Kim S-W (2007) A three-probe system for measuring the parallelism and straightness of a pair of rails for ultra-precision guideways. Int J Mach Tools Manuf 47:1053–1058
7. Donaldson RR (1972) A simple method for separating spindle error from test ball roundness error. Ann CIRP 21:125–126
8. Estler WT (1985) Calibration and use of optical straightedges in the metrology of precision machines. Opt Eng 24:372–379
9. Evans CJ, Hocken RJ, Estler WT (1996) Self-calibration: reversal, redundancy, error separation, and absolute testing. Ann CIRP 45:617–634
10. Tanaka H, Tazawa K, Sato H, O-hori M, Sekiguchi H (1981) Application of a new straightness measurement method to large machine tools. Ann CIRP 30:455–459
11. Tazawa K, Sato H, O-hori M (1982) A new method for the measurement of the straightness of machine tools and machined work. ASME J Mech Des 104:587–592
12. Kiyono S, Gao W (1994) Profile measurement of machined surface with a new differential method. Precis Eng 16:212–218
13. Gao W, Kiyono S (1996) High accuracy profile measurement of a machined surface by the combined method. Measurement 19:55–64
14. Makosch G, Drollinger B (1984) Surface profile measurement with a scanning differential ac interferometer. Appl Opt 23–24:4544–4553
15. Tanaka H, Sato H (1986) Extensive analysis and development of straightness measurement by sequential two-point method. Trans ASME 108:176–182
16. Park CH, Lee H (2004) Motion error analysis of the porous air bearing stage using the transfer function. Journal of the Korean Society of Precision Engineering 21:185–194
17. Hwang J, Park C-H, Lee C-H, Kim S-W (2006) Estimation and correction method for the two-dimensional position errors of a planar *XY* stage based on motion error measurements. Int J Mach Tools Manuf 46:801–810
18. Okafor AC, Ertekin YM (2000) Derivation of machine tool error models and error compensation procedure for three axes vertical machining. Int J Mach Tools Manuf 40:1199–1213
19. Raksiri C, Parnichkun M (2005) Geometric and force errors compensation in a 3-axis CNC milling machine. Int J Mach Tools Manuf 44:1283–1291
20. Slocum AH (1992) Precision machine design. Prentice Hall, Englewood Cliffs, NJ